Applied Clay Science 246 (2023) 107163

Contents lists available at ScienceDirect

Applied Clay Science

journal homepage: www.elsevier.com/locate/clay

Research Paper

UV-cured gel polymer electrolytes based on poly (ethylene glycol) and organo-modified nanoclays for lithium ions batteries

Ernestino Lufrano [a], Luigi Coppola [a], Isabella Nicotera [a,b], Cataldo Simari [a,b,*]

[a] Department of Chemistry and Chemical Technologies, University of Calabria, 87036 Rende, Italy
[b] National Reference Centre for Electrochemical Energy Storage (GISEL)—INSTM, Via G. Giusti 9, 50121 Firenze, Italy

ARTICLE INFO

Keywords:
lithium ions batteries
Gel polymer electrolytes
Montmorillonite
Nanocomposite GPEs
^{7}Li NMR
Safe GPEs

ABSTRACT

Next-generation electrolytes for Lithium Ion Batteries (LIBs) must provide increased durability, reliability, safety, and scalability to meet the even more stringent technical requirements of crucial industries such as e-mobility. A promising strategy to merge these technical needs is the development of easy-to-prepare gel polymer electrolytes (GPEs) able to ensure satisfactory conductivity, high stability, and reduced flammability. In this study, we propose the preparation of novel nanocomposite GPEs through one-pot in-situ photo-polymerization (UV-curing), which turns out to be of great interest due to its low-cost, solvent-free and energy-saving characteristics. Poly (ethylene glycol) dimethacrylate (PEG-DMA) was used as hosting polymer matrix, while 1 M Lithium bis (trifluoromethanesulfonyl) imide (LiTFSI) in ethylene carbonate/dimethyl carbonate (EC/DMC) was used as electrolyte solution. Organo-modified montmorillonite (fMt, intercalated with CTAB) was synthesized and tested as a nanofiller. Both materials and GPEs were characterized by a combination of experimental techniques including FTIR, XRD, SEM, and DMA. Noteworthy, a thorough and systematic study of the lithium-ion transport properties in the prepared GPEs was carried out using pulsed-field gradient nuclear magnetic resonance (PFG-NMR) and electrochemical impedance spectroscopy (EIS). This preliminary study demonstrated the gP-fMt combines ease of preparation and excellent safety (i.e., thermomechanical stability up to 250 °C and nonflammability) with satisfactory lithium transport properties.

1. Introduction

Current Lithium Ion Batteries (LIBs) are still reliant on flammable organic solvents, which pose risks of leakage and associated fire hazards. To address these concerns, the development of solid-state devices emerges as one of the most promising strategies for creating high-performance, safe, and stable energy storage and conversion devices (PbSO et al., 2008). In this context, gel polymer electrolytes (GPEs) have garnered rapid attention from researchers worldwide in the pursuit of designing low-cost and secure rechargeable LIBs. This is due to their ability to combine satisfactory ion conductivity with robust mechanical strength, adaptable geometry, absence of liquid leakage, and consequently, heightened safety (Song et al., 1999). De facto, GPEs possess the cohesive properties of solids alongside the diffusive characteristics of liquids. The synthetic approach is quite straightforward and involves the incorporation of a liquid solution (generally obtained by dissolution of the appropriate lithium salt in a mixture of carbonate solvents) into a host polymeric systems containing -E(thylene)O(xide)- moieties (Stephan, 2006). To date, various polymeric materials have been reported and tested as polymer hosts, including poly (ethylene oxide) (PEO), poly (acrylonitrile) (PAN), poly (methyl methacrylate) (PMMA), and poly (vinylidene fluoride-hexafluoro propylene) (PVdF-HFP), etc. (Nicotera et al., 2004, 2006; Simari et al., 2018). However, though some of these systems demonstrated quite high ionic conductivities at room temperature (10^{-4}–10^{-3} S cm^{-1}), their poor mechanical strength as well as the low thermal and flame resistance still hinder the large-scale diffusion of current GPEs (Xue et al., 2015; Tsurumaki et al., 2019).

An alternative and innovative approach, namely the free-radical photopolymerization, has recently gained great interest as it proves to be a low-cost, solvent-free and energy-saving technique (Crivello and Reichmanis, 2014; Shao et al., 2014). Indeed, the UV-induced reaction on multifunctional monomers allows for rapid in situ generation of polymer electrolytes which are highly homogeneous in terms of both morphology and dimensionality, thus enabling perfect electrode/electrolyte interfaces (Griffini et al., 2015). Furthermore, the entire electrolyte preparation can be carried out in the absence of solvent. Among

* Corresponding author at: Department of Chemistry and Chemical Technologies, University of Calabria, 87036 Rende, Italy.
E-mail address: cataldo.simari@unical.it (C. Simari).

https://doi.org/10.1016/j.clay.2023.107163
Received 7 July 2023; Received in revised form 11 October 2023; Accepted 11 October 2023
Available online 16 October 2023

the multitude of available monomers, poly (ethylene glycol) (PEG) functionalized with methacrylate groups appears to be of great interest for the development of GPEs (Armand, 1983; Javadi et al., 2016). Such polymers can be polymerized to form graft structures comprising a carbon-carbon backbone and multiple side chains of oligo(ethylene glycol) segments, or to create a cross-linked network if both ends are functionalized by methacrylate via a rapid UV-curing process (Javadi et al., 2016). Similar to other monomers or oligomers, PEG methacrylate can be synthesized to various molecular weights to generate products with different cross-link densities and corresponding properties, such as stiffness, swelling, porosity, modulus, etc. (Fairbanks et al., 2009; Hume et al., 2011).

In this work, in situ photopolymerization of Poly(ethylene glycol) dimethacrylate (PEG-DMA) has been employed for the preparation of new polymeric gel electrolytes through an easily reproducible and safe procedure. PEG-DMA was used as the hosting polymer matrix capable of encapsulating an electrolyte solution based on a lithium salt (LiTFSI) dissolved in carbonate solvents (ethylene carbonate and dimethyl carbonate). Importantly, for the first time, the UV-curing and the nanocomposite approaches were combined to maximize the overall performance of the PEG-based GPEs. The development of composite electrolytes represents an interesting subset of the preparation of GPEs, which relies on the incorporation of electrochemically inert fillers into polymer matrices (Simari et al., 2016; Enotiadis et al., 2018; Lufrano et al., 2020; Rehman et al., 2023). Typically, high surface area particulate fillers such as ZrO_2, TiO_2, Al_2O_3, and hydrophobic fumed silica are incorporated into the polymer matrices to reduce the crystallinity of the resulting GPEs (thereby increasing their ionic conductivity) while simultaneously enhancing the mechanical resistance (Croce et al., 1998). More recently, it has been demonstrated that smectite nanomaterials can noticeably enhance ionic conductivity at low temperatures as well as improve stability at the interface with electrodes (Simari et al., 2018). Consequently, herein, an organo-modified montmorillonite (fMt) has been prepared and investigated as a filler. The organo-clay was prepared by intercalation of CTAB molecules in the interlamellar space of Mt. material through a cation-exchange reaction. The organo-modification is expected to increase the affinity with both the polymer matrix and the carbonate plasticizers, thus reducing the leaching risk as well as increasing the flame-retardant features of the nanocomposite GPEs. Morphological, structural, mechanical, and thermal properties of both filler and GPEs were thoroughly investigated using a combination of experimental techniques including SEM, XRD, FTIR, and DMA. Flammability tests were carried out to demonstrate the impressive safety feature of the nanocomposite GPEs, while a thorough and systematic study of the lithium-ion transport was conducted on the prepared GPEs using pulsed-field gradient nuclear magnetic resonance (PFG-NMR) and electrochemical impedance spectroscopy (EIS).

2. Results and discussion

2.1. Organophilic-montmorillonite (fMt)

Fig. 1(a) illustrates the XRD profiles of the Mt. (in its lithium form) and organo-functionalized Mt., from now on fMt. The XRD pattern of Mt. exhibits the typical features of basic montmorillonite structure with a single broad diffraction peak (d_{001}) relating to a basal spacing at ≈11.8 Å. The latter is clearly amenable to the presence of the Li^+ cations as the main counterbalancing ions in the interlayer space of the Mt. structure. In the case of fMt, the 2θ angle shifts from 7.17° (as in the case of Mt) till 3.62° that is a basal spacing of ≈ 25.6 Å which corresponds to a paraffin-type monolayer structure (Zhu et al., 2003). The evidence suggests CTAB ions were successfully intercalated in the silicate layers of Mt., resulting in the organophilic montmorillonites. Additionally, FTIR analysis was carried out to further confirm the opportune modification of Mt. In this regard, Fig. 1(b) compares the FTIR spectra of both Mt. and fMt materials. Montmorillonite exhibits a main broad band at ca. 1010 cm^{-1} with a small peak at 920 cm^{-1} and two less intense signals at 1160 cm^{-1} and 793 cm^{-1} which are all characteristic absorption bands related to stretching vibrations of Si—O and Al—O (Sarier et al., 2010). Comparatively, the FTIR spectrum of fMt shows three additional bands which are not distinct in Li—Mt. In particular, the peaks at 2920 cm^{-1} and 2850 cm^{-1} can be assigned to the -CH_2 symmetrical and asymmetrical stretching vibrations of CTAB while the absorbance band at 1470 cm^{-1} is attributed to stretching vibrations of -CH_3 groups due to the presence of quaternary ammonium salt (Vaia et al., 1994).

Finally, the morphology of Mt. and its derivative was investigated by Scanning Electron Microscopy (SEM) and the resulting images reported in Fig. 2. Clearly, CTAB intercalation only involves the interlayer space between the Mt. lamellae. Consequently, the materials exhibit very similar morphology characterized by small platelets stacked to form a grain, which is characteristic of the layered structure of montmorillonite (Sarier et al., 2010). Despite this, one can still detect a slight difference between organophilic-Mt (Fig. 2b) and parental Mt. (Fig. 2a): silica platelets are closer in the case of pristine Mt. whereas are more separated as well as disposed as flakes in the case of CTAB-Mt (Barkoula et al., 2008; Simari et al., 2018). According to the literature, the phenomenon is clearly amenable to the organophilization of Mt. materials which affects both the surface and the interlayer space of the clays and in turns reduces the hydrophilicity of the material (Chen et al., 2014).

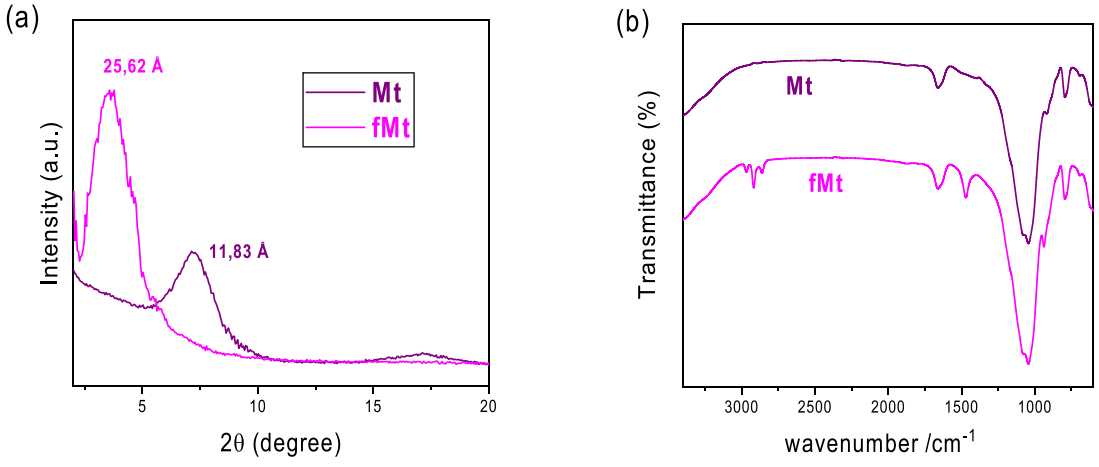

Fig. 1. (a) XRD profiles and (b) FTIR spectra of monmorillonite (Mt) and its organophilic derivative (fMt).

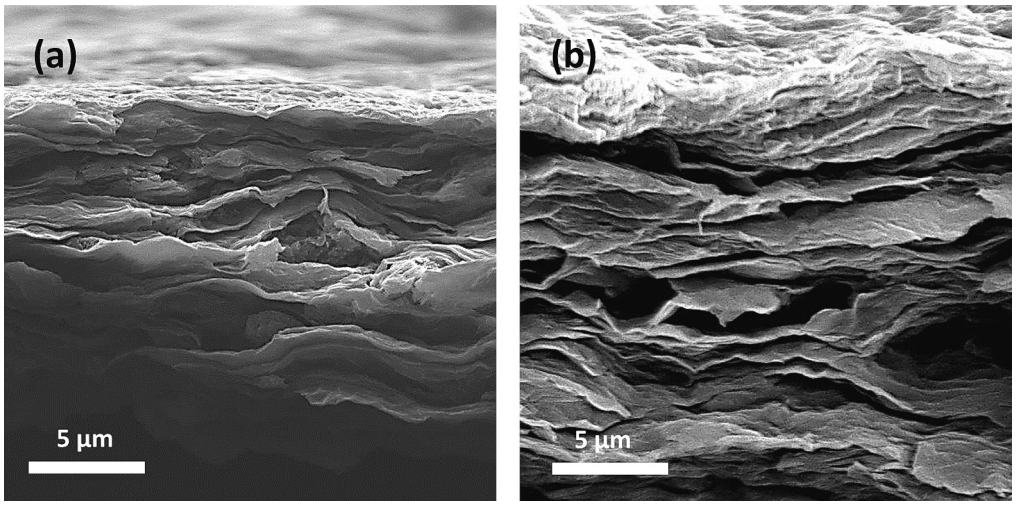

Fig. 2. SEM images of (a) Montmorillonite and (b) organophilic Montmorillonite.

2.2. PEG-based gel polymer electrolytes

Following the successful synthesis of organophilic-Mt, the nanomaterial was used as nanoadditive for the preparation of PEG-based nanocomposite GPEs. SEM analysis was also employed to clarify morphological features of the prepared gels. Fig. 3 shows the SEM images of gPEG, gP-Mt and gP-fMt cross-sections obtained during criofracturing. Bare gPEG exhibits a dense and compact structure without any clear evidence of holes or pores. The introduction of both Mt. and fMt materials does not alter the microstructure of the GPEs, which maintain a uniform cross-section. However, while qP-Mt exhibits some small agglomerates through its cross-section, the gP-fMt membranes is highly homogeneous indicating the organo-modified clay particles maintain sub-micrometric dimensions. The evidence suggests organophilization of Mt. materials increases the chemical affinity between the filler and the PEG polymer chains allowing to obtain a composite membrane characterized by a real nanodispersion. The presence of Mt. and fMt nanoparticles in the PEG matrix was confirmed by FTIR investigation. In fact, the main absorption bands of both gPEG polymer and parental nanomaterial coexist in the FTIR spectra of the nanocomposite membranes (refer to fig. S1). This proves the successful incorporation of the montmorillonite nanoparticles in the PEG matrix.

Typically, the presence of the liquid carbonate solvents limits the mechanical resistance of the GPEs. However, our gPEG-based composite electrolytes hold promise for outstanding mechanical strength since combines a solid-like nature with high flexibility (see Fig. 11). Characterization of mechanical features of the GPEs systems was carried out by Dynamic Mechanical Analysis (DMA) under shear configuration. Fig. 4 shows the temperature evolution, in the range 20–300 °C, of storage modulus (E') and dumping factor (tan δ) for the various gels. Bare gPEG already exhibits an impressive mechanical resistance with its storage modulus of 4.3×10^7 Pa, which is one of the highest values reported for literature GPEs (Nicotera et al., 2004; Ramesh and Liew, 2012; Enotiadis et al., 2018). This might be ascribed to the UV-curing process which likely enables high rigidity of the system. Noteworthy, the addition of Mt. platelets in the PEG matrix has beneficial effect on the its thermomechanical performance. Indeed, nanocomposite GPEs are characterized by a noticeable increase in the storage modulus as well as a considerable temperature extension of the mechanical resistance. The phenomenon is clearly amenable to the polymer reinforcing capability of 2D-layered clay material (Nicotera et al., 2019; Simari et al., 2020, 2021c; Poiana et al., 2021). As above mentioned, organo-modification of Mt. promotes favourable interaction between the polymer chains and the clay platelets. Consequently, the best results were observed on gP-fMt: such GPE is able to ensure superior mechanical strength (i.e., ca. 1.0×10^8 Pa) without dimensional changes and/or physical deterioration up to 200 °C. The dumping factor plot (Fig. 4b) better elucidates the effect of the Mt. nanoparticles on the thermal stability of the resulting GPEs. One can clearly notice that glass transition temperature (T_g) remarkably increases after introduction of the cationic clay, from the initial value of 216 °C in the case of pristine gPEG till 267 °C on the gP-fMt nanocomposite. De facto, thermomechanical resistance of the proposed electrolytes significantly exceed the typical operating temperature of LIBs, thus decreasing the safety risk.

To gain further insights on the safety of Mt-based membranes, a flammability test was carried out, as shown in Fig. 5. Because of the presence of EC/DMC liquid mixture, gPEG burns immediately after ignition and keeps combusting even after the flame is removed. Opposite

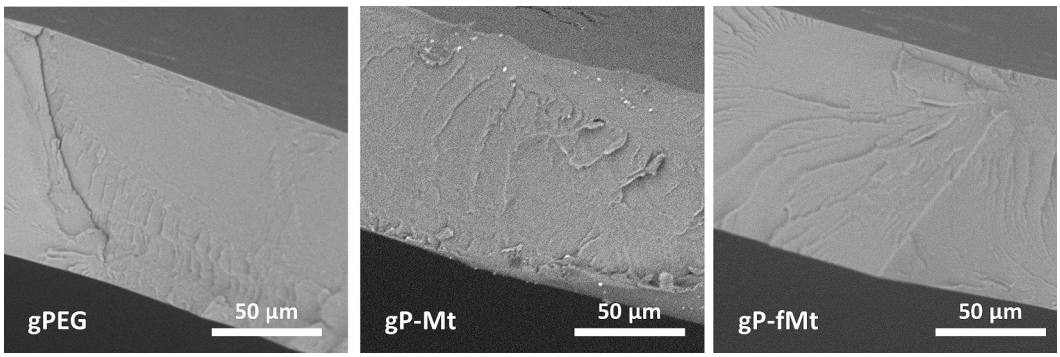

Fig. 3. Cross-sectional SEM images of the gPEG-based electrolytes.

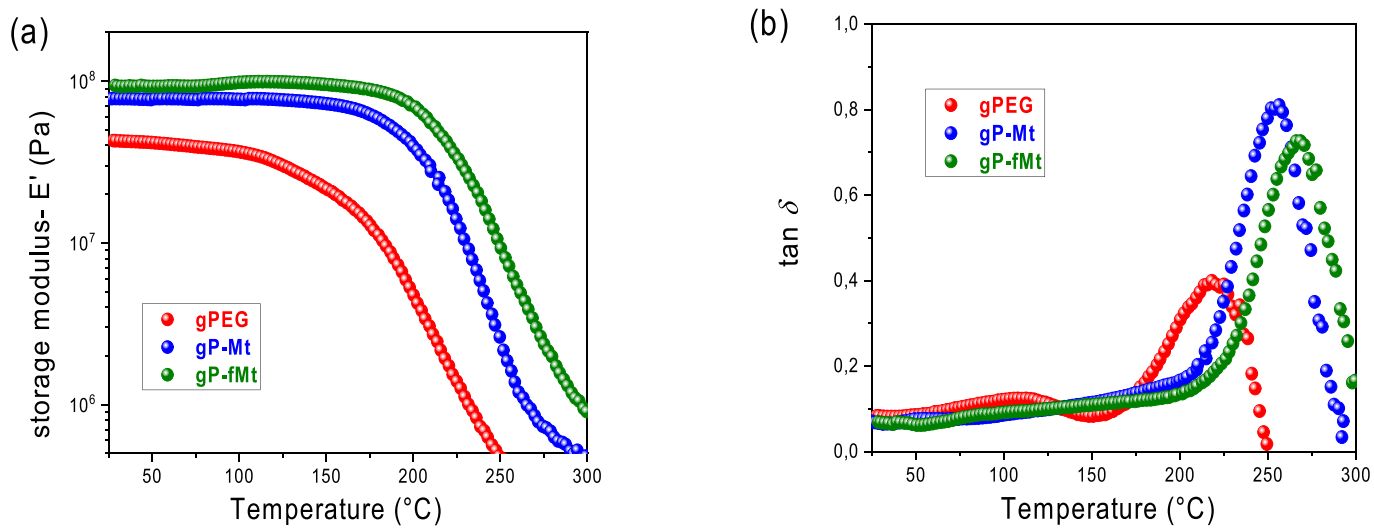

Fig. 4. Temperature evolution of the (a) storage modulus *E'* and (b) Tan δ for gPEG and nanocomposite membranes containing Mt. materials. gP-Mt = nanocomposite gel containing pristine montmorillonite; gP-fMt = nanocomposite with organomodified montmorillonite.

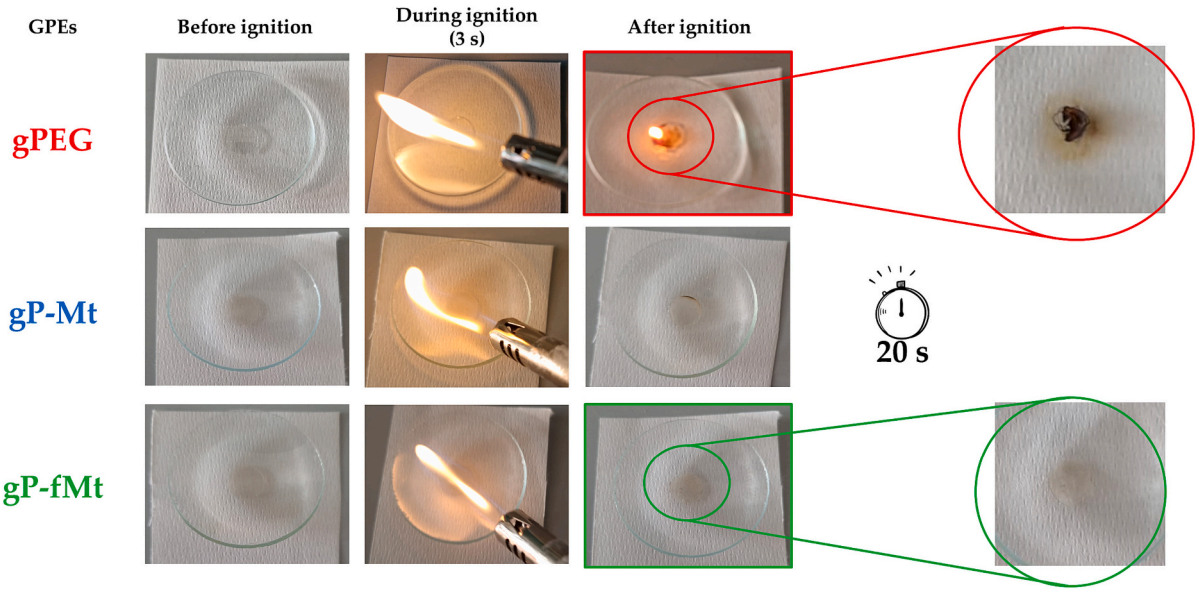

Fig. 5. Flammability test of the PEG-based gel polymer electrolytes. With Mt. = montmorillonite material and fMt = organomodified montmorillonite material.

of that, the gP-Mt does not catch a fire after ignition but only a very small burned area is observed on the membrane surface. Noteworthy, an even superior resistance to flammability is evidenced in the case of gP-fMt. The feature can be likely ascribed to the strong ability of the organophilic Mt. in retaining liquid electrolytes which in turn results in an impressive safety improvement for such nanocomposite GPEs.

Finally, to estimate their real suitability for practical application, gel polymer electrolytes must ensure two crucial features such as high ion diffusivity and ionic conductivity. Consequently, the parameters were deeply analysed based on the PFG-NMR investigation and EIS measurements, respectively. The PFG NMR technique is a powerful method to directly and individually measure the self-diffusion coefficients of diffusing species (Kidd et al., 2015; Nicotera et al., 2015, 2017; D'Angelo and Panzer, 2018; Munoz and Greenbaum, 2018; Tsurumaki et al., 2019; Simari et al., 2021a) including EC/DMC mixture (D_H), lithium ions (D_{Li}) and hexafluorophosphate anions (D_F). Fig. 6 illustrates the diffusivity data for lithium and its counterion collected in the temperature range from 20 °C to 80 °C. Lithium self-diffusion coefficients significantly increases after introduction of Mt. nanoparticles. Aluminosilicate platelets are characterized by a fixed negative charge which enables the filler particles to be directly in the Li^+ transport mechanism. Consequently, the gP-Mt exhibits the highest diffusivity among the GPEs achieving 1.8×10^{-7} cm^2 s^{-1} at 80 °C. Following the intercalation of CTAB molecules, the Mt. becomes more organophilic. De facto, carbonates solvents experiences stronger interactions with the fMt lamellae which in turns slightly decreases the lithium mobility due to a slower vehicular mechanism. Turing the attention on ^{19}F nucleus, the mobility of $TFSI^-$ ions is almost one order of magnitude higher than the lithium one in the case of bare PEG. For instance, at 20 °C D_F is 1.19×10^{-7} cm^2 s^{-1} while D_{Li} is 1.2×10^{-8} cm^2 s^{-1}. It has been widely demonstrated that $TFSI^-$ ions weakly interact with the ethylene oxide moieties of both the PEG matrix and carbonates sorbents (Orädd et al., 2002; Devaux et al., 2012; Falco et al., 2019). This induces faster diffusion characteristics for $TFSI^-$ ions compared to Li^+ ions. Wort noting, the introduction of Mt. produces a marked reduction of the counterion mobility, which even more pronounced in the case of gP-fMt. Such behaviour provides clear

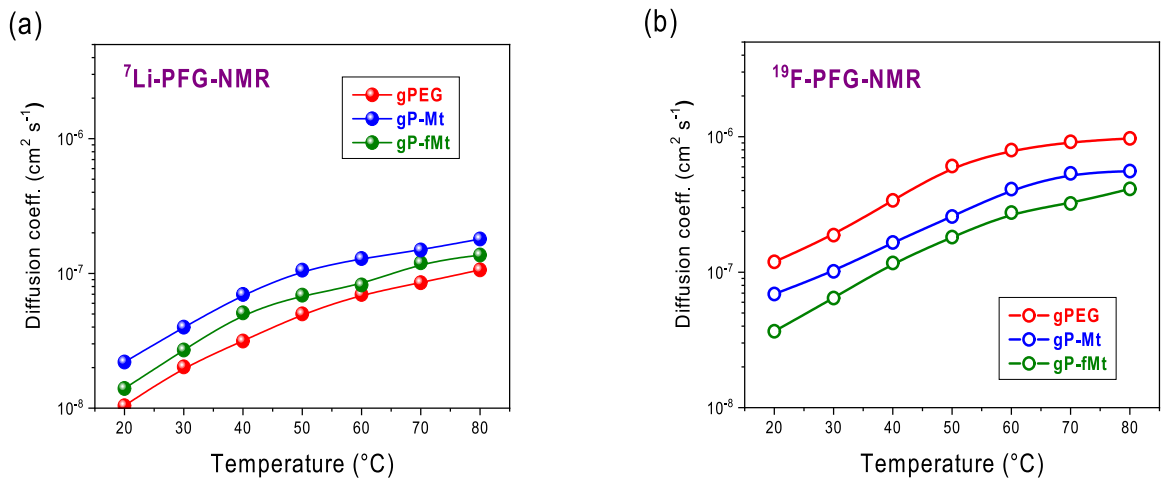

Fig. 6. Temperature variation, in the range 20–80 °C, of the self-diffusion coefficients for (a) Li^+ (^{7}Li) and (b) counterion (^{19}F) measured on gPEG and nanocomposite electrolytes.

indication that 2D nanoplatelets is able to considerably reduce the mobility of bulkier $TFSI^-$ ions likely due to an increase in the tortuosity of its diffusional paths. Obviously, the introduction of long alkyl chains as in the case of fMt further exacerbates this phenomenon.

Self-diffusion coefficient values were then used to calculate another important parameter for GEPs, namely the apparent transference numbers (t_{Li+}), which relates to the individual contribution of the cations and anions to the overall ionic conductivity of the gel electrolyte (Zewde et al., 2018). The t_{Li+} was calculated according to the following Eq. (1) and reported in Table 1:

$$t_{Li^+} = \frac{D_{Li^+}}{D_{Li^+} + D_{F^-}} \quad (1)$$

The gPEG electrolyte exhibits a t_{Li+} value of 0.08 at r.t., much lower than characteristic values for literature GPEs, for which values close to 0.30 are generally reported (Gorecki et al., 1995; Castriota et al., 2003; Zhang et al., 2014; Zhao et al., 2016; Zewde et al., 2018). This suggest that both cation and anion equally contribute to the ion conducting performance of the pristine electrolyte. However, it is worth pointing out that the presence of Mt. and fMt in the gels produces an appreciable increase in t_{Li+}, and the highest average value is found for the gP-fMt sample, i.e. ca. 0.28. The reasons of this phenomenon can be multiple and synergistic: (i) due to the layered structure the Mt. particles decrease the overall mobility of bulky $TFSI^-$; and (ii) electrostatic interactions between the filler surface and lithium likely promotes the formation of preferential pathways for lithium conduction.

The latter speculation was further corroborated by the NMR longitudinal (or spin-lattice) relaxation time, T_1, which quantifies the energy transfer rate from the nuclear spin system to the nearby molecules (the lattice). Unlike the self-diffusion coefficient, T_1 reflects more localized motions, encompassing both translation and rotation, occurring on a time scale equivalent to the reciprocal of the NMR angular frequency (few nanoseconds). The stronger the interactions, the lower the molecular mobility resulting in quicker relaxation times (shorter T_1). Fig. 7 illustrates the temperature evolution in spin-lattice relaxation of ^{19}F and ^{7}Li, for all the GPEs. It is evident that the T_1 values for ^{19}F nuclei decrease in the order gPEG > gP-Mt > gP-fMt, confirming that Mt. nanoparticles obstruct $TFSI^-$ mobility even at molecular scale. Conversely, the incorporation of Mt. materials leads to higher Li^+ T_1 values, promoting greater molecular mobility. This underscores that the negatively charged platelets enhance lithium transport, likely through a hopping mechanism.

To demonstrate the promising prospects of gP-fMt as a scalable and safe gel polymer electrolyte for low-temperature lithium batteries, the ionic conductivity (σ) was investigated using EIS. Fig. 8 displays the Arrhenius plot of the σ measured in the temperature range 20–80 °C for the gPEG-based electrolyte membranes. All GPEs exhibit ionic conductivity well above 0.1 mS cm^{-1} at room temperature, perfectly meeting the performance requirements for practical applications in LIBs. Table 2 provides a performance comparison with literature GPEs for further context. In addition, conductivity increases with rising temperature, as the flexibility of polymer chains progressively improves during heating, leading to more efficient ion transport (Vasile et al., 2017; Quartarone et al., 2023). Specifically, the conductivity for pristine gPEG ranges from 0.19 mS cm^{-1} at 20 °C to 0.40 mS cm^{-1} at 80 °C, which is slightly higher than literature value for PEG-based gel electrolytes (Jin et al., 2022). Likely, the UV curing reduces the crystalline phase of gPEG thus enabling higher σ. Furthermore, lithium conductivity increases after the incorporation of Mt. nanoparticles, as negatively charged lamellae are directly involved in the transport mechanism of Li^+ ions. As a result, gP-Mt exhibits the best performance among the investigated GPEs, yielding a conductivity of 0.49 mS cm^{-1} at 80 °C, which represents a 22% of improvement compared to gPEG. On the contrary, the incorporation of organophilic Mt. has a detrimental effect on lithium conduction. As above mentioned, the long alkyl chains of fMt nanoparticles facilitate stronger interactions between clay platelets and the carbonate solvents, which slows down the rate of lithium conduction trough vehicular mechanism. However, when comparing the Activation Energy (E_A) values, calculated from a linear fit of the Arrhenius plots for the three samples, it is evident that gP-fMt has the lowest E_A, specifically 8.95 kJ mol^{-1}. This clearly indicates a more efficient ionic transfer process.

Table 1
Apparent lithium transport number for gPEG, gPEG-Montmorillonite (gP-Mt) and gPEG-organophilic montmorillonite (gP-fMt) electrolytes in the temperature range 20–80 °C.

T [°C]	t_{Li+}		
	gPEG	gP-Mt	gP-fMt
20	0.08	0.24	0.28
30	0.10	0.28	0.30
40	0.08	0.30	0.30
50	0.08	0.29	0.28
60	0.08	0.24	0.23
70	0.09	0.22	0.27
80	0.10	0.24	0.25

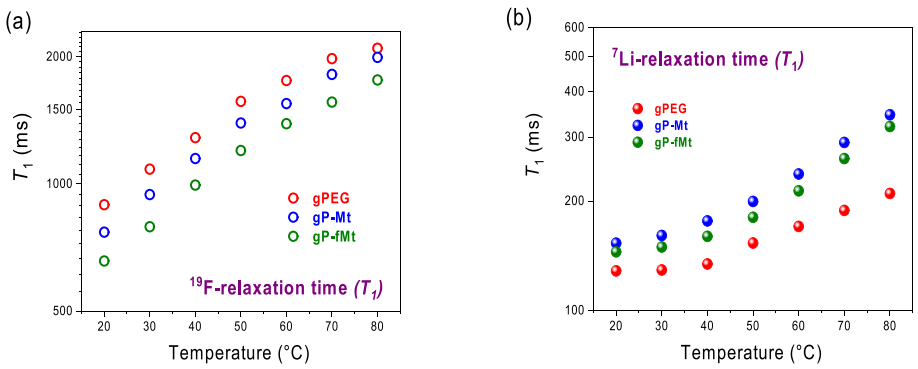

Fig. 7. (a) ^{19}F and (b) ^{7}Li spin-lattice relaxation times (T_1) vs. temperature, in the range 20–80 °C for gPEG, gPEG-Montmorillonite (gP-Mt) and gPEG-organophilic montmorillonite (gP-fMt) electrolytes.

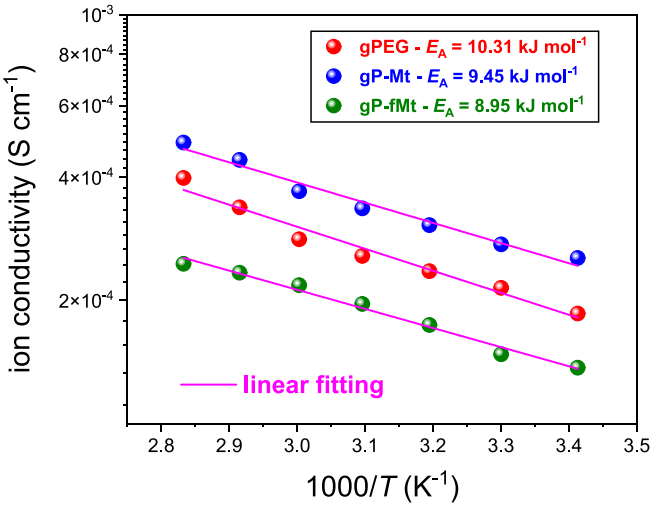

Fig. 8. Arrhenius plots of ionic conductivities measured on gPEG-based electrolytes, were gP-Mt is the nanocomposite gel containing pristine Montmorillonite and gP-fMt is the electrolytes incorporating organophilic montmorillonite. Solid pink lines represent the linear fitting to experimental data. (For interpretation of the references to colour in this figure legend, the reader is referred to the web version of this article.)

3. Materials and methods

3.1. Materials

Polyethylene glycol di-methacrylate (PEGDMA, average Mw 600), Lithium bis(trifluoromethanesulfonyl) imide (LiTFSI), Ethylene carbonate (EC, 98%), Dimethyl carbonate (DMC, 99%), 2,2 dimethoxy-2-phenylacetophenone (Irgacure 641, 99%) and Lithium hydroxide (LiOH, 98%) were purchased from Aldrich and used as received. Natural smectite Wyoming montmorillonite (Mt) has obtained from the Source Clay Minerals Repository, University of Missouri, Columbia. The structural formula is $Na_{0.62}[Al_{3.01}Fe\ (III)_{0.41}Mg_{0.54}Mn_{0.01}Ti_{0.02}]\ (Si_{7.98}Al_{0.02})O_{20}(OH)_4$.

3.2. Synthesis of lithiated organo-modified Montmorillonite (fMt—Li+)

The Mt. in sodic form was first fractioned to <2 μm through gravity sedimentation and subsequently purified using well-established procedures in clay science (Nicotera et al., 2012). Subsequently, the clay was converted to its lithium form via an ion exchange process with a 2 M lithium hydroxide solution at room temperature for 48 h, replacing the LiOH solution multiple times. The resulting lithiated Mt. powder was collected by centrifugation, underwent repeated rinses with deionized water, and was then dried for 24 h at 90 °C. The ion exchange between sodium and lithium did not result in any alteration of the chemical structure of Mt., as proved by FTIR analysis (see Fig. S2 in Supporting Information) but only a small reduction in the basal spacing (see Fig. S3 in Supporting Information). For the chemical modification, the cation exchange capacity of smectite clay has been exploited according to a standard procedure as schematized in Fig. S4. CTAB (0.4 g) was dissolved in boiling deionized water until complete dissolution. Subsequently, the resulting solution as added dropwise, with vigorous stirring, to a dispersion of SWy-2 (1.0 g) in deionized water at 60 °C, and left for 6 h to achieve complete cationic exchange. Finally, the mixture solution was separated by centrifugation, rinsed repeatedly with deionized water until Br^- was completely removed, and finally dried for 24 h at 90 °C.

3.3. Preparation of cross-linked solid polymer electrolytes

Gel polymer electrolytes based on PEG were obtained by UV-induced radical polymerization without the use of any organic solvent. The procedure is schematized in Fig. 9. For the bare PEG electrolyte (from now on gPEG), the appropriate amount of PEGDMA precursor, EC/DMC liquid electrolyte mixture, LiTFSI lithium salt as Li^+ ions source, and 2,2 dimethoxy-2-phenylacetophenone (Ir641) as a photo-initiator were mixed and left under stirring for 10 min at room temperature. Thereafter, the solution was cast and sandwiched between two glass plates separated by a spacer with 80 μm thickness, which corresponds to the final thickness of the prepared GPEs. Finally, it was photo-crosslinked through UV irradiation for 10 min under UVA lamp (254 nm). The final gel polymer electrolytes films were peeled off from the glass plate and directly used for characterization. The nanocomposite membranes with Mt. (referred to as gP-Mt) and organophilic-Mt (referred to as gP-fMt) were prepared with the same procedure, with the direct addition of the appropriate amount of filler to the polymer solution, followed by vigorous stirring at room temperature for 2 h. Filler content was kept at 10 wt% with respect to the polymer amount. The entire procedure was performed in glove box, under nitrogen atmosphere.

3.4. Characterization techniques

NMR measurements were performed on a Bruker NMR spectrometer AVANCE 300 Wide Bore working at 300 MHz on ^{1}H, 116.6 MHz on ^{7}Li, and 282.4 MHz on ^{19}F, respectively. The employed probe was a Diff30 *Z*-diffusion 30 G/cm/A multinuclear with substitutable RF inserts. ^{1}H, ^{7}Li, and ^{19}F self-diffusion coefficients and spin-lattice relaxation times were taken at different temperatures, from 20 °C up to 80 °C, in 10 °C intervals. The sample was allowed to equilibrate at each temperature for approximately 20 min. For the self-diffusion coefficient measurements, the pulsed field gradient stimulated echo (PFG-STE) method was employed (Tanner, 1970). The sequence consists of three 90° RF pulses ($\pi/2$-$\tau 1$-$\pi/2$-τm-$\pi/2$) and two gradient pulses that are applied after the

Table 2
Some GPEs researched in the recent years and their physicochemical and electrochemical properties.

GPEs	Method preparation	Ionic Conductivity @ 25 °C (mS / cm)	t^+	Reference
gP-Mt	Photo polymerization	0.25	0.24	This work
gP-fMt		0.14	0.28	
SPE-PEGDMA$_{480}$	Photo polymerization	0.24	0.27	(Wei et al., 2019)
PEGDMA-SO_3Li/TEGME	Photo polymerization	0.11	0.28	(Ma et al., 2016)
PVDF/LiPVAOB	Electrospinning	0.26	0.58	(Zhu et al., 2014)
BEMA/PEGMA	Photo polymerization	0.84	0.42	(Chiappone et al., 2011)
PAMM	Thermochemical crosslinking/AIBN	0.68		(Ma et al., 2017)
PTHF	Polymerization	0.23	0.36	(Huang et al., 2019)
P(PEGMA/GO-STTA0.5%)	Thermally activated RAFT polymerization	0.55	0.61	(Hamrahjoo et al., 2022)
PEGMA-SPE_4	Photo polymerization	0.02		(Nair et al., 2011)
CPE-3	Photo polymerization	0.35	0.47	(Ahmed et al., 2021)
POM	Thermochemical polymerization	0.11		(Wu et al., 2020)
PVDF/Graphene	Non-solvent induced phase separation (NIPS)	0.36	0.59	(Liu et al., 2017)
PVDF-HFP	Solution casting	0.37	0.58	(Liang et al., 2018)
MC	Solution casting	0.2	0.29	(Xiao et al., 2014)
PPU5	Photo polymerization	1.88	0.62	(Siccardi et al., 2022)
SISPEs-3	Photo polymerization	1.03	0.36	(Rong et al., 2022)
PEG_{400}/SiO_2	Solution casting	0.39		(Xu et al., 2016)
PEO-PMMA/Al_2O_3	Solution casting	9.37×10^{-4}	0.1	(Liang et al., 2015)
PMMA-PEO/SiO_2	Solution casting	0.26		(Yap et al., 2019)
Cellulose/TPU	Photo polymerization	0.23	0.68	(Bao et al., 2017)

SPE = solid polymer electrolyte; TEGME = Triethylene glycol methyl ether; PVDF = polyvinylidene difluoride; BEMA = Behenyl Methacrylate; PEGMA = Poly (ethylene glycol) methacrylate; PAMM = Polyacrylamide; PTHF = Polytetrahydrofuran; CPE = Cross-linked polymer electrolytes; POM = Polyoxometalate; HFP = Hexafluoropropylene; PPU = copolymer of PEGMEM, PEGDA575 and UpyMa; SISPEs = semi-interpenetrating solid state polymer networks electrolytes; PMMA-PEO = copolymer of polymethyl methacrylate and Polyethylene oxide; TPU = Thermoplastic polyurethane.

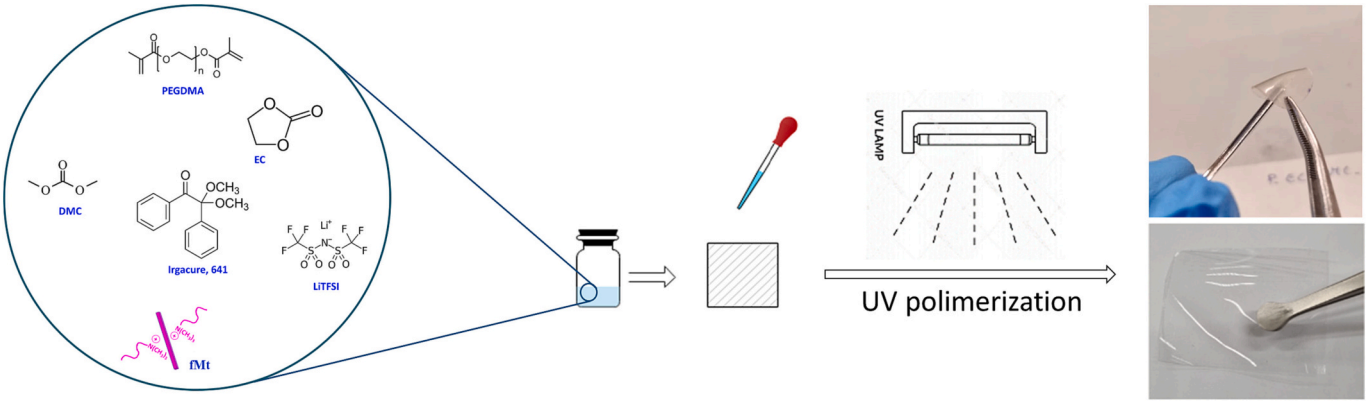

Fig. 9. Schematic representation of the synthetic procedure for PEG-based gel electrolytes. On the right rise, two real pictures of a freshly prepared electrolyte. EC = Ethylene carbonate; DMC = Dimethyl carbonate, PEGDMA = Polyethylene glycol di-methacrylate; LiTFSI = Lithium bis(trifluoromethanesulfonyl) imide.

first and the third RF pulses, respectively. The echo is registered at time $\tau = 2\tau_1 + \tau m$. Using the standard notation, the magnetic field pulses have magnitude g, duration δ, and time delay Δ. The FT echo decays were analysed by means of the Stejskal–Tanner expression (Eq. 2):

$$I = I_0\, e^{-\beta D} \tag{2}$$

Where the parameters I and I_0 represent the intensity/area of selected resonance peaks in the presence and in absence of gradients, respectively. Instead β is the field gradient parameter, defined as $\beta = [(\gamma g \delta)^2 \times (\Delta - \delta/3)]$ and D is the measured self-diffusion coefficient. For the investigated samples, the used experimental parameters were: $\delta = 3$ ms, time delay $\Delta = 30$ ms, and the gradient amplitude varied from 350 to 1000G cm^{-1}. Due to the very low standard deviation of the fitting curve and repeatability of the measurements, the uncertainties in the self-diffusion measurements are approximately 3%. Finally, longitudinal or spin-lattice relaxation times (T_1) were measured by the inversion-recovery sequence ($\pi - \tau - \pi/2$).

The ionic conductivity (σ, S cm^{-1}) was measured by Electrochemical Impedance Spectroscopy (EIS) using a two-electrodes AC impedance method in the temperature range 20–80 °C (Simari et al., 2021d). The complex impedance measurements were recorded with an oscillating potential of 10 mV in the frequency range 0.1 Hz – 1 MHz using a PGSTAT 30 (Metrohm-Autolab) potentiostat/galvanostat/FRA. Samples were sandwiched between two stainless steels electrodes and assembled in a commercial two-electrode cell (ECC-Std electrochemical cell). The membrane resistance (R) was extracted from the intercept of the high-frequency semicircle in the corresponding Nyquist plot, and its conductivity was calculated by Eq. (3).

$$\sigma = \frac{L}{R \bullet S} \tag{3}$$

where L is the membrane thickness and S is the active surface.

The mechanical properties were investigated using Dynamic Mechanical Analysis (DMA) conducted on a Metravib DMA/25 analyser equipped with a shear jaw for films clamping (Simari et al., 2021b). The measurements were performed on rectangular-shaped samples (35 mm × 10 mm). Frequency sweep experiments were carried out in the frequency range between 0.2 and 20 Hz at a constant strain of 0.004%, from 20 °C to 80 °C every 10 °C (Enotiadis et al., 2017). Temperature sweep tests were performed at a heating rate of 2 °C, over a range

between 20 °C and 120 °C, at a dynamic stress with an amplitude 4×10^{-3} and frequency of 1 Hz.

The FTIR spectra were recorded in the range 400–3600 cm^{-1} using a Perkin-Elmer Spectrum GX instrument with KBr pellets for powdered samples whereas circularly shaped samples were directly cut from the GPEs (Callegari et al., 2021). Each spectrum was the average of 128 scans collected at 2 cm^{-1} resolutions, and these were further averaged to enhance the signal-to-noise ratio.

4. Conclusions

A new class of nanocomposite Gel Polymer Electrolytes based on Poly (ethylene glycol) and organo-modified nanoclays has been developed using a cost-effective, solvent-free, and energy-efficient technique, i.e., UV-induced photopolymerization. The organophilic montmorillonite material (fMt) was prepared through a straightforward cation-exchange reaction, involving the intercalation of CTAB molecules within the interlamellar space of Mt. XRD analysis and SEM images revealed an increase in the basal spacing of Mt. following the incorporation of CTAB while the presence of characteristic absorption bands of CTAB in the FTIR profile of fMt definitely confirmed the successful organophilization of Mt. materials. Due to the favourable interaction between the polymer chains and the fMt platelets, the gP-fMt nanocomposite displayed impressive mechanical resistance, i.e., 1.0×10^8 Pa of storage modulus, without any physical deterioration till almost 250 °C. Furthermore, such nanocomposite membrane balanced at the best satisfactory electrochemical performance with superior safety. The organo-modified Mt. promotes lithium mobility while restricting the movements of $TFSI^-$ counterion. Consequently, gP-fMt exhibited the highest lithium transport number (t_{Li+}) among the samples with a conductivity of ca. 0.4 mS cm^{-1} at room temperature. On the other side, the organophilic Mt. material allows to retain liquid carbonates inside the GPEs, implying gP-fMt did not catch a fire after ignition during flammability tests. The results demonstrated that the gP-fMt has the potential to be used as a gel polymer electrolytes for safer LIBs.

Funding

This research received no external funding.

CRediT authorship contribution statement

Ernestino Lufrano: Investigation, Data curation, Writing – original draft. **Luigi Coppola:** Validation, Investigation, Writing – original draft. **Isabella Nicotera:** Conceptualization, Methodology, Validation, Resources, Project administration, Funding acquisition. **Cataldo Simari:** Conceptualization, Validation, Formal analysis, Data curation, Writing – original draft, Writing – review & editing, Visualization, Supervision.

Declaration of Competing Interest

The authors declare no conflict of interest.

Data availability

No data was used for the research described in the article.

Appendix A. Supplementary data

Supplementary data to this article can be found online at https://doi.org/10.1016/j.clay.2023.107163.

References

Ahmed, F., Kim, D., Lei, J., Ryu, T., Yoon, S., Zhang, W., Lim, H., Jang, G., Jang, H., Kim, W., 2021. UV-cured cross-linked astounding conductive polymer electrolyte for safe and high-performance, batteries. ACS Appl. Mater. Interfaces 13, 34102–34113. https://doi.org/10.1021/acsami.1c06233.

Armand, M., 1983. Polymer solid electrolytes - an overview. Solid State Ionics 9–10, 745–754. https://doi.org/10.1016/0167-2738(83)90083-8.

Bao, J.J., Zou, B.K., Cheng, Q., Huang, Y.P., Wu, F., Xu, G.W., Chen, C.H., 2017. Flexible and free-standing LiFePO4/TPU/SP cathode membrane prepared via phase separation process for lithium ion batteries. J. Membr. Sci. 541, 633–640. https://doi.org/10.1016/j.memsci.2017.06.083.

Barkoula, N.M., Alcock, B., Cabrera, N.O., Peijs, T., 2008. Flame-retardancy properties of intumescent ammonium poly(phosphate) and mineral filler magnesium hydroxide in combination with graphene. Polym. Polym. Compos. 16, 101–113. https://doi.org/10.1002/pc.

Callegari, D., Colombi, S., Nitti, A., Simari, C., Nicotera, I., Ferrara, C., Mustarelli, P., Pasini, D., Quartarone, E., 2021. Autonomous self-healing strategy for stable sodium-ion battery: a case study of black phosphorus anodes. ACS Appl. Mater. Interfaces 13, 13170–13182. https://doi.org/10.1021/acsami.0c22464.

Castriota, M., Cazzanelli, E., Nicotera, I., Coppola, L., Oliviero, C., Ranieri, G.A., 2003. Temperature dependence of lithium ion solvation in ethylene carbonate-LiClO4 solutions. J. Chem. Phys. 118, 5537–5541. https://doi.org/10.1063/1.1528190.

Chen, S., Zhou, W., Cao, Y., Xue, C., Lu, C., 2014. Organo-modified montmorillonite enhanced chemiluminescence via inactivation of halide counterions in a micellar solution. J. Phys. Chem. C 118, 2851–2856. https://doi.org/10.1021/jp411290z.

Chiappone, A., Nair, J.R., Gerbaldi, C., Jabbour, L., Bongiovanni, R., Zeno, E., Beneventi, D., Penazzi, N., 2011. Microfibrillated cellulose as reinforcement for Li-ion battery polymer electrolytes with excellent mechanical stability. J. Power Sources 196, 10280–10288. https://doi.org/10.1016/j.jpowsour.2011.07.015.

Crivello, J.V., Reichmanis, E., 2014. Photopolymer materials and processes for advanced technologies. Chem. Mater. 26, 533–548. https://doi.org/10.1021/cm402262g.

Croce, F., Appetecchi, G.B., Persi, L., Scrosati, B., 1998. Nanocomposite polymer electrolytes for lithium batteries. Nature 394, 456–458. https://doi.org/10.1038/28818.

D'Angelo, A.J., Panzer, M.J., 2018. Decoupling the ionic conductivity and elastic modulus of gel electrolytes: fully zwitterionic copolymer scaffolds in lithium salt/ionic liquid solutions. Adv. Energy Mater. 8, 1–13. https://doi.org/10.1002/aenm.201801646.

Devaux, D., Bouchet, R., Glé, D., Denoyel, R., 2012. Mechanism of ion transport in PEO/LiTFSI complexes: effect of temperature, molecular weight and end groups. Solid State Ionics 227, 119–127. https://doi.org/10.1016/j.ssi.2012.09.020.

Enotiadis, A., Boutsika, L.G., Spyrou, K., Simari, C., Nicotera, I., 2017. A facile approach to fabricating organosilica layered material with sulfonic groups as an efficient filler for polymer electrolyte nanocomposites. New J. Chem. 41 https://doi.org/10.1039/c7nj01416c.

Enotiadis, A., Fernandes, N.J., Becerra, N.A., Zammarano, M., Giannelis, E.P., 2018. Nanocomposite electrolytes for lithium batteries with reduced flammability. Electrochim. Acta 269, 76–82. https://doi.org/10.1016/j.electacta.2018.02.079.

Fairbanks, B.D., Schwartz, M.P., Bowman, C.N., Anseth, K.S., 2009. Photoinitiated polymerization of PEG-diacrylate with lithium phenyl-2,4,6-trimethylbenzoylphosphinate: polymerization rate and cytocompatibility. Biomaterials 30, 6702–6707. https://doi.org/10.1016/j.biomaterials.2009.08.055.

Falco, M., Simari, C., Ferrara, C., Nair, J.R., Meligrana, G., Bella, F., Nicotera, I., Mustarelli, P., Winter, M., Gerbaldi, C., 2019. Understanding the effect of UV-Induced Cross-linking on the Physicochemical Properties of Highly performing PEO/LiTFSI-Based Polymer Electrolytes. Langmuir. https://doi.org/10.1021/acs.langmuir.9b00041 acs.langmuir.9b00041.

Gorecki, W., Jeannin, M., Belorizky, E., Roux, C., Armand, M., 1995. Physical properties of solid polymer electrolyte PEO(LiTFSI) complexes. J. Phys. Condens. Matter 7, 6823–6832. https://doi.org/10.1088/0953-8984/7/34/007.

Griffini, G., Bella, F., Nisic, F., Dragonetti, C., Roberto, D., Levi, M., Bongiovanni, R., Turri, S., 2015. Multifunctional luminescent down-shifting fluoropolymer coatings: a straightforward strategy to improve the UV-light harvesting ability and long-term outdoor stability of organic dye-sensitized solar cells. Adv. Energy Mater. 5, 1–9. https://doi.org/10.1002/aenm.201401312.

Hamrahjoo, M., Hadad, S., Dehghani, E., Salami-Kalajahi, M., Roghani-Mamaqani, H., 2022. Preparation of matrix-grafted graphene/poly(poly(ethylene glycol) methyl ether methacrylate) nanocomposite gel polymer electrolytes by reversible addition-fragmentation chain transfer polymerization for lithium ion batteries. Eur. Polym. J. 176, 111419 https://doi.org/10.1016/j.eurpolymj.2022.111419.

Huang, S., Cui, Z., Qiao, L., Xu, G., Zhang, J., Tang, K., Liu, X., Wang, Q., Zhou, X., Zhang, B., Cui, G., 2019. An in-situ polymerized solid polymer electrolyte enables excellent interfacial compatibility in lithium batteries. Electrochim. Acta 299, 820–827. https://doi.org/10.1016/j.electacta.2019.01.039.

Hume, P.S., Bowman, C.N., Anseth, K.S., 2011. Functionalized PEG hydrogels through reactive dip-coating for the formation of immunoactive barriers. Biomaterials 32, 6204–6212. https://doi.org/10.1016/j.biomaterials.2011.04.049.

Javadi, A., Mehr, H.S., Sobani, M., Soucek, M.D., 2016. Cure-on-command technology: a review of the current state of the art. Prog. Org. Coat. 100, 2–31. https://doi.org/10.1016/j.porgcoat.2016.02.014.

Jin, L., Jang, G., Lim, H., Zhang, W., Park, S., Jeon, M., Jang, H., Kim, W., 2022. Improving the ionic conductivity of PEGDMA-based polymer electrolytes by reducing the interfacial resistance for LIBs. Polymers (Basel) 14. https://doi.org/10.3390/polym14173443.

Kidd, B.E., Forbey, S.J., Steuber, F.W., Moore, R.B., Madsen, L.A., 2015. Multiscale lithium and counterion transport in an electrospun polymer-gel electrolyte. Macromolecules 48, 4481–4490. https://doi.org/10.1021/acs.macromol.5b00573.

Liang, B., Tang, S., Jiang, Q., Chen, C., Chen, X., Li, S., Yan, X., 2015. Preparation and characterization of PEO-PMMA polymer composite electrolytes doped with nano-

Al2O3. Electrochim. Acta 169, 334–341. https://doi.org/10.1016/j.electacta.2015.04.039.
Liang, Y.F., Deng, S.J., Xia, Y., Wang, X.L., Xia, X.H., Wu, J.B., Gu, C.D., Tu, J.P., 2018. A superior composite gel polymer electrolyte of Li7La3Zr2O12- poly(vinylidene fluoride-hexafluoropropylene) (PVDF-HFP) for rechargeable solid-state lithium ion batteries. Mater. Res. Bull. 102, 412–417. https://doi.org/10.1016/j.materresbull.2018.02.051.
Liu, J., Wu, X., He, J., Li, J., Lai, Y., 2017. Preparation and performance of a novel gel polymer electrolyte based on poly(vinylidene fluoride)/graphene separator for lithium ion battery. Electrochim. Acta 235, 500–507. https://doi.org/10.1016/j.electacta.2017.02.042.
Lufrano, E., Simari, C., Lo Vecchio, C., Aricò, A.S., Baglio, V., Nicotera, I., 2020. Barrier properties of sulfonated polysulfone/layered double hydroxides nanocomposite membrane for direct methanol fuel cell operating at high methanol concentrations. Int. J. Hydrog. Energy 45, 20647–20658. https://doi.org/10.1016/j.ijhydene.2020.02.101.
Ma, L., Nath, P., Tu, Z., Tikekar, M., Archer, L.A., 2016. Highly conductive, sulfonated, UV-cross-linked separators for Li-S batteries. Chem. Mater. 28, 5147–5154. https://doi.org/10.1021/acs.chemmater.6b02190.
Ma, Y., Ma, J., Chai, J., Liu, Z., Ding, G., Xu, G., Liu, H., Chen, B., Zhou, X., Cui, G., Chen, L., 2017. Two players make a formidable combination: in situ generated poly (acrylic anhydride-2-methyl-acrylic acid-2-oxirane-ethyl ester-methyl methacrylate) cross-linking gel polymer electrolyte toward 5 v high-voltage batteries. ACS Appl. Mater. Interfaces 9, 41462–41472. https://doi.org/10.1021/acsami.7b11342.
Munoz, S., Greenbaum, S., 2018. Review of recent nuclear magnetic resonance studies of ion transport in polymer electrolytes. Membranes (Basel) 8, 1–23. https://doi.org/10.3390/membranes8040120.
Nair, J.R., Gerbaldi, C., Destro, M., Bongiovanni, R., Penazzi, N., 2011. Methacrylic-based solid polymer electrolyte membranes for lithium-based batteries by a rapid UV-curing process. React. Funct. Polym. 71, 409–416. https://doi.org/10.1016/j.reactfunctpolym.2010.12.007.
Nicotera, I., Coppola, L., Oliviero, C., Russo, A., Ranieri, G.A., 2004. Some physicochemical properties of PAN-based electrolytes: solution and gel microstructures. Solid State Ionics 167, 213–220. https://doi.org/10.1016/j.ssi.2003.09.007.
Nicotera, I., Coppola, L., Oliviero, C., Castriota, M., Cazzanelli, E., 2006. Investigation of ionic conduction and mechanical properties of PMMA-PVdF blend-based polymer electrolytes. Solid State Ionics 177, 581–588. https://doi.org/10.1016/j.ssi.2005.12.028.
Nicotera, I., Enotiadis, A., Angjeli, K., Coppola, L., Gournis, D., 2012. Evaluation of smectite clays as nanofillers for the synthesis of nanocomposite polymer electrolytes for fuel cell applications. Int. J. Hydrog. Energy 37, 6336–6345. https://doi.org/10.1016/j.ijhydene.2011.06.041.
Nicotera, I., Kosma, V., Simari, C., Ranieri, G.A., Sgambetterra, M., Panero, S., Navarra, M.A., 2015. An NMR study on the molecular dynamic and exchange effects in composite Nafion/sulfated titania membranes for PEMFCs. Int. J. Hydrog. Energy 40, 14651–14660. https://doi.org/10.1016/j.ijhydene.2015.06.137.
Nicotera, I., Simari, C., Boutsika, L.G., Coppola, L., Spyrou, K., Enotiadis, A., 2017. NMR investigation on nanocomposite membranes based on organosilica layered materials bearing different functional groups for PEMFCs. Int. J. Hydrog. Energy 42. https://doi.org/10.1016/j.ijhydene.2017.05.014.
Nicotera, I., Simari, C., Agostini, M., Enotiadis, A., Brutti, S., 2019. A Novel Li + − Na fi on-sulfonated graphene oxide membrane as single lithium-ion conducting polymer electrolyte for lithium batteries. J. Phys. Chem. C 123, 27406–27416. https://doi.org/10.1021/acs.jpcc.9b08826.
Orädd, G., Edman, L., Ferry, A., 2002. Diffusion: a comparison between liquid and solid polymer LiTFSI electrolytes. Solid State Ionics 152–153, 131–136. https://doi.org/10.1016/S0167-2738(02)00364-8.
PbSO, P., Koh, N., Li, E., Si, V., LiX, S., 2008. PbO 2 H 2 O H 2 SO 4 /H 2 O H + PbSO 4 SO 4 2−+−e-2.0 V Lead-acid Li 1-x CoO 2 LiPF 6 EC-DMC LiPF 6 EC-DMC Lithium ion Future batteries? Lithium ion based on nanomaterials Ionic liquids Lithium metal Lithium-air Lithium-based electrolytes. Nature 451, 652–657.
Poiana, R., Lufrano, E., Tsurumaki, A., Simari, C., Nicotera, I., Navarra, M.A., 2021. Safe gel polymer electrolytes for high voltage Li-batteries. Electrochim. Acta 401, 139470. https://doi.org/10.1016/j.electacta.2021.139470.
Quartarone, E., Davino, S., Lufrano, E., Coppola, L., Simari, C., Nicotera, I., 2023. Ions dynamics and diffusion in self-healing chemical gel electrolytes for Li-ion batteries. ChemElectroChem. https://doi.org/10.1002/celc.202201148.
Ramesh, S., Liew, C.W., 2012. Rheological characterizations of ionic liquid-based gel polymer electrolytes and fumed silica-based composite polymer electrolytes. Ceram. Int. 38, 3411–3417. https://doi.org/10.1016/j.ceramint.2011.12.053.
Rehman, M.H.U., Lufrano, E., Simari, C., 2023. Nanocomposite membranes for PEM-FCs: effect of LDH introduction on the physic-chemical performance of various polymer matrices. Polymers (Basel) 15, 502. https://doi.org/10.3390/polym15030502.
Rong, Z., Sun, Y., Zhao, Q., Cheng, F., Zhang, W., Chen, J., 2022. UV-cured semi-interpenetrating polymer networks of solid electrolytes for rechargeable lithium metal batteries. Chem. Eng. J. 437, 135329 https://doi.org/10.1016/j.cej.2022.135329.
Sarier, N., Onder, E., Ersoy, S., 2010. The modification of Na-montmorillonite by salts of fatty acids: an easy intercalation process. Colloids Surf. A Physicochem. Eng. Asp. 371, 40–49. https://doi.org/10.1016/j.colsurfa.2010.08.061.
Shao, J., Huang, Y., Fan, Q., 2014. Visible light initiating systems for photopolymerization: Status, development and challenges. Polym. Chem. 5, 4195–4210. https://doi.org/10.1039/c4py00072b.
Siccardi, S., Amici, J., Colombi, S., Carvalho, J.T., Versaci, D., Quartarone, E., Pereira, L., Bella, F., Francia, C., Bodoardo, S., 2022. UV-cured self-healing gel polymer electrolyte toward safer room temperature lithium metal batteries. Electrochim. Acta 433. https://doi.org/10.1016/j.electacta.2022.141265.
Simari, C., Potsi, G., Policicchio, A., Perrotta, I., Nicotera, I., 2016. Clay−carbon nanotubes hybrid materials for nanocomposite membranes: advantages of branched structure for proton transport under low humidity conditions in PEMFCs. J. Phys. Chem. C 120, 2574–2584. https://doi.org/10.1021/acs.jpcc.5b11871.
Simari, C., Lufrano, E., Coppola, L., Nicotera, I., 2018. Composite gel polymer electrolytes based on organo-modified nanoclays: Investigation on lithium-ion transport and mechanical properties. Membranes (Basel) 8. https://doi.org/10.3390/membranes8030069.
Simari, C., Lo Vecchio, C., Baglio, V., Nicotera, I., 2020. Sulfonated polyethersulfone/polyetheretherketone blend as high performing and cost-effective electrolyte membrane for direct methanol fuel cells. Renew. Energy 159, 336–345. https://doi.org/10.1016/j.renene.2020.06.053.
Simari, C., Lufrano, E., Brunetti, A., Barbieri, G., Nicotera, I., 2021a. Polysulfone and organo-modified graphene oxide for new hybrid proton exchange membranes: a green alternative for high-efficiency PEMFCs. Electrochim. Acta 380, 138214. https://doi.org/10.1016/j.electacta.2021.138214.
Simari, C., Lufrano, E., Lemes, G., Lázaro, M.J., Sebastián, D., Nicotera, I., 2021b. Electrochemical performance and alkaline stability of cross-linked quaternized polyepichlorohydrin/PvDF blends for anion-exchange membrane fuel cells. J. Phys. Chem. C 125, 5494–5504. https://doi.org/10.1021/acs.jpcc.0c11346.
Simari, C., Lufrano, E., Rehman, M.H.U., Zhegur-Khais, A., Haj-Bsoul, S., Dekel, D.R., Nicotera, I., 2021c. Effect of LDH platelets on the transport properties and carbonation of anion exchange membranes. Electrochim. Acta 403, 139713. https://doi.org/10.1016/j.electacta.2021.139713.
Simari, C., Prejanò, M., Lufrano, E., Sicilia, E., Nicotera, I., 2021d. Exploring the structure–performance relationship of sulfonated polysulfone proton exchange membrane by a combined computational and experimental approach. Polymers (Basel) 13, 959. https://doi.org/10.3390/polym13060959.
Song, J.Y., Wang, Y.Y., Wan, C.C., 1999. Review of gel-type polymer electrolytes for lithium-ion batteries. J. Power Sources 77, 183–197. https://doi.org/10.1016/S0378-7753(98)00193-1.
Stephan, A.M., 2006. Review on gel polymer electrolytes for lithium batteries. Eur. Polym. J. 42, 21–42. https://doi.org/10.1016/j.eurpolymj.2005.09.017.
Tanner, J.E., 1970. Use of the stimulated echo in NMR diffusion studies. J. Chem. Phys. 52, 2523–2526.
Tsurumaki, A., Agostini, M., Poiana, R., Lombardo, L., Lufrano, E., Simari, C., Matic, A., Nicotera, I., Panero, S., Navarra, M.A., 2019. Enhanced safety and galvanostatic performance of high voltage lithium batteries by using ionic liquids. Electrochim. Acta 316, 1–7. https://doi.org/10.1016/j.electacta.2019.05.086.
Vaia, R.A., Teukolsky, R.K., Giannelis, E.P., 1994. Interlayer structure and molecular environment of alkylammonium layered silicates. Chem. Mater. 6, 1017–1022. https://doi.org/10.1021/cm00043a025.
Vasile, N.S., Monteverde Videla, A.H.A., Simari, C., Nicotera, I., Specchia, S., 2017. Influence of membrane-type and flow field design on methanol crossover on a single-cell DMFC: an experimental and multi-physics modeling study. Int. J. Hydrog. Energy 42, 27995–28010. https://doi.org/10.1016/j.ijhydene.2017.06.214.
Wei, Z., Zhang, Z., Chen, S., Wang, Z., Yao, X., Deng, Y., Xu, X., 2019. UV-cured polymer electrolyte for LiNi0.85Co0.05Al0.1O2//Li solid state battery working at ambient temperature. Energy Storage Mater. 22, 337–345. https://doi.org/10.1016/j.ensm.2019.02.004.
Wu, H., Tang, B., Du, X., Zhang, Jianjun, Yu, X., Wang, Y., Ma, J., Zhou, Q., Zhao, J., Dong, S., Xu, G., Zhang, Jinning, Xu, H., Cui, G., Chen, L., 2020. LiDFOB initiated in situ polymerization of novel eutectic solution enables room-temperature solid lithium metal batteries. Adv. Sci. 7, 1–9. https://doi.org/10.1002/advs.202003370.
Xiao, S., Wang, F., Yang, Y., Chang, Z., Wu, Y., 2014. An environmentally friendly and economic membrane based on cellulose as a gel polymer electrolyte for lithium ion batteries. RSC Adv. 4, 76–81. https://doi.org/10.1039/c3ra46115g.
Xu, J., Li, J., Zhu, Y., Zhu, K., Liu, Y., Liu, J., 2016. A triPEG-boron based electrolyte membrane for wide temperature lithium ion batteries. RSC Adv. 6, 20343–20348. https://doi.org/10.1039/c6ra02865a.
Xue, Z., He, D., Xie, X., 2015. Poly(ethylene oxide)-based electrolytes for lithium-ion batteries. J. Mater. Chem. A 3, 19218–19253. https://doi.org/10.1039/c5ta03471j.
Yap, Y.L., You, A.H., Teo, L.L., 2019. Preparation and characterization studies of PMMA–PEO-blend solid polymer electrolytes with SiO2 filler and plasticizer for lithium ion battery. Ionics (Kiel) 25, 3087–3098. https://doi.org/10.1007/s11581-019-02842-8.
Zewde, B.W., Carbone, L., Greenbaum, S., Hassoun, J., 2018. A novel polymer electrolyte membrane for application in solid state lithium metal battery. Solid State Ionics 317, 97–102. https://doi.org/10.1016/j.ssi.2017.12.039.
Zhang, H., Liu, C., Zheng, L., Xu, F., Feng, W., Li, H., Huang, X., Armand, M., Nie, J., Zhou, Z., 2014. Lithium bis(fluorosulfonyl)imide/poly(ethylene oxide) polymer electrolyte. Electrochim. Acta 133, 529–538. https://doi.org/10.1016/j.electacta.2014.04.099.
Zhao, Y., Huang, Z., Chen, S., Chen, B., Yang, J., Zhang, Q., Ding, F., Chen, Y., Xu, X., 2016. A promising PEO/LAGP hybrid electrolyte prepared by a simple method for all-solid-state lithium batteries. Solid State Ionics 295, 65–71. https://doi.org/10.1016/j.ssi.2016.07.013.
Zhu, J., He, H., Guo, J., Yang, D., Xie, X., 2003. Arrangement models of alkylammonium cations in the interlayer of HDTMA + pillared montmorillonites. Chin. Sci. Bull. 48, 368–372. https://doi.org/10.1360/03tb9078.
Zhu, Y., Xiao, S., Shi, Y., Yang, Y., Hou, Y., Wu, Y., 2014. A composite gel polymer electrolyte with high performance based on poly(vinylidene fluoride) and polyborate for lithium ion batteries. Adv. Energy Mater. 4, 1–9. https://doi.org/10.1002/aenm.201300647.